Journal of Solid State Chemistry **158,** 100–111 (2001)
doi:10.1006/jssc.2000.9105, available online at http://www.idealibrary.com on IDEAL®

Synthesis and Crystal Structure of Novel Layered Manganese Oxide $Ca_2MnGaO_{5+\delta}$

A. M. Abakumov,[1] M. G. Rozova, B. Ph. Pavlyuk, M. V. Lobanov, and E. V. Antipov

Department of Chemistry, Moscow State University, Moscow 119899, Russia

O. I. Lebedev[2] and G. Van Tendeloo

EMAT, University of Antwerp (RUCA), Groenenborgerlaan 171, B-2020 Antwerp, Belgium

D. V. Sheptyakov and A. M. Balagurov

Frank Laboratory of Neutron Physics, JINR, 141980 Dubna, Russia

and

F. Bourée

Laboratoire Léon Brillouin, CEA-CNRS, CE-Saclay, 91191 Gif-sur-Yvette, France

Received October 10, 2000; in revised form January 3, 2001; accepted January 19, 2001

New layered oxides $Ca_2MnGaO_{5+\delta}$ and $Ca_2MnGa_{1-x}Zn_xO_{5+\delta}$ ($x = 0.1$, 0.2) were synthesized by solid-state reaction at 1000–1300°C. The crystal structure of $Ca_2MnGaO_{5.045}$ was studied using X-ray, neutron and electron diffraction, and high-resolution electron microscopy (HREM). The samples of $Ca_2MnGaO_{5.045}$ consist of two closely intermixed brownmillerite-type phases with *Pnma* or *Ima*2 space symmetry that possess very closely related structures that differ mainly by the orientation of the Ga–O chains. The formal Mn valence (V_{Mn}) in $Ca_2MnGaO_{5+\delta}$ can be varied either by heterovalent replacement of Ga^{3+} for Zn^{2+} or by oxygen insertion after treatment under 80 atm O_2. In the latter case the compound with the composition $Ca_2MnGaO_{5.39}$ forms built of domains of initial reduced material and fully oxidized $Ca_2MnGaO_{5.5}$ phase. The $Ca_2MnGaO_{5.5}$ structure was determined by HREM as belonging to the brownmillerite $A_nB_{n-1}B'O_{3n-1}$ ($n = 4$) homologous series, in which three layers of BO_6 (B = Mn, Ga) octahedra form blocks separated by a single layer of $B'O_4$ (B' = Ga) tetrahedra. The increase of V_{Mn} from +3.09 to +3.78 is accompanied by a drastic compression of the structure along the $b = 4a_{per}$ axis due to a suppression of the Jahn-Teller deformation of the MnO_6 octahedra. © 2001 Academic Press

[1] To whom correspondence should be addressed. E-mail: abakumov@icr.chem.msu.ru. Fax: (095) 939-47-88.

[2] On leave from Institute of Crystallography, RAS, Leninsky pr. 59, 117333 Moscow, Russia.

Key Words: **$Ca_2MnGaO_{5+\delta}$; synthesis; crystal structure; oxygen nonstoichiometry.**

1. INTRODUCTION

The effect of colossal magnetoresistance (CMR) (1) in complex manganese oxides has attracted considerable attention in recent years. Nevertheless the research has been mostly confined to a narrow group of compounds, mainly three-dimensional perovskites, $AMnO_{3-\delta}$, in which the optimum charge carrier concentration was achieved by heterovalent substitution on the A sublattice. Investigations on other classes of compounds embrace an intermediate case of dimensionality between $D = 3$ in perovskites and $D = 2$ in the structures built up by alternating perovskite layers and rock-salt-type blocks of different thickness. The members of Ruddlesden–Popper series with the general formula $A_{n+1}Mn_nO_{3n+1}$ (A = rare-earth or alkaline-earth cations) exhibit CMR at appropriate doping level (2, 3). The general trend is a decrease of both Curie temperature (T_c) and metal–insulator transition temperature (T_p) and a concomitant increase in magnetoresistanse (MR) upon lowering the dimensionality (2). The $Bi_{2-x}Pb_xSr_2MnO_{6+\delta}$ ($x = 0$, 1) (4, 5) and $Bi_{2-x}Pb_xSr_{1.5}Ca_{1.5}Mn_2O_{9-\delta}$ (6) oxides provide examples of structures where single or double (MnO_2) layers are separated by four-layer rock-salt slabs;

0022-4596/01 $35.00

they are isotypic with the $Bi_2Sr_2Ca_{n-1}Cu_nO_{2n+4+\delta}$ superconductors. These compounds are antiferromagnetic and the CMR properties were not reported for a wide range of Mn formal valence ($+2.6-+3.3$, as evaluated by thermogravimetry) (7).

The layered perovskite-like structure can also arise from an ordered distribution of two types of *B*-cations with clearly distinct coordination environment. Anion-deficient ordered double perovskites $A_2BB'O_5$ (*B*, transition metal cation, *B'*, cation with tetrahedral coordination (Al, Ga)) with a brownmillerite-type structure can be described as a stacking sequence of layers:

$$-(BO_2)-(AO)-(B'O\square)-(AO)-(BO_2)- .$$

B atoms are located in BO_6 octahedra sharing common corners; they form layers separated by $B'O_4$ tetrahedra. The $B'O_4$ tetrahedra are also interconnected into chains by corner sharing. The 10-fold cavities in the structure are occupied by *A* cations. The compounds with such a structure could possibly provide another realization of a two-dimensional Mn–O matrix and are plausible to exhibit CMR properties at an appropriate doping level. It may be achieved either by heterovalent substitution or by a variation of oxygen stoichiometry that is accessible due to an incomplete oxygen sublattice. Having in mind the similarity between crystal chemistry properties of Mn^{3+} and Cu^{2+} cations, one can assume that Mn-based analogs of La*A*-$CuGaO_5$ (*A* = Ca, Sr) brownmillerites (8, 9) could also be synthesized. The goal of the present work is the preparation of Ca_2MnGaO_5 brownmillerite with a variable Mn formal valence and the investigation of its crystal structure.

2. EXPERIMENTAL

Samples with nominal compositions Ca_2MnGaO_5 and $Ca_2MnGa_{1-x}Zn_xO_5$ ($x = 0.1$, 0.2, 0.3) were prepared by solid-state reactions using $CaCO_3$, CaO, Mn_2O_3, MnO_2, Ga_2O_3, and ZnO as initial reagents. The synthetic routes listed below were tested to achieve the best quality of the samples:

(i) stoichiometric amounts of CaO (prepared by decomposition of $CaCO_3$ in dynamic vacuum at 900°C), Mn_2O_3, and Ga_2O_3 were ground in an agate mortar in a glove box free of H_2O and CO_2. The mixture was placed in an alumina crucible, sealed in an evacuated silica tube, and annealed at 1000°C for 8 days with one intermediate regrinding. After annealing the samples were quenched.

(ii) a stoichiometric mixture of $CaCO_3$, MnO_2, and Ga_2O_3 was pressed into a pellet and annealed at 1000°C for 50 h and then reground and annealed at 1200–1300°C in air. This technique was applied for the preparation of Zn-substituted compounds as well.

(iii) a stoichiometric mixture of $CaCO_3$, MnO_2, and Ga_2O_3 was annealed at 800°C in air and at 1100–1200°C for 40–120 h in nitrogen flow.

Additional thermal treatments under high oxygen pressure (20–80 atm, 415–430°C) were carried out to investigate the variation of oxygen content and Mn oxidation state. The annealings were performed in a hermetic stainless steel autoclave. The Mn formal valence in as-prepared and in oxidized samples was determined by iodometric titration.

Phase analysis and cell parameter determination was performed using X-ray powder diffraction with a focusing Guinier-camera FR-552 ($CuK\alpha_1$-radiation, Ge was used as an internal standard). X-ray powder diffraction data for crystal structure determination were collected on a STADI-P diffractometer ($CuK\alpha_1$-radiation, curved Ge monochromator, transmission mode, linear PSD). RIETAN-97 program was used for the Rietveld refinement of the structure from X-ray diffraction data (10). For the final structure refinement, a neutron powder diffraction (NPD) experiment was performed with the 3T2 diffractometer at Laboratoire Leon Brillouin, Saclay ($\lambda = 1.225$ Å). Rietveld refinements were carried out using the FullProf program.

Electron diffraction (ED) and high-resolution electron microscopy (HREM) studies were performed using a JEOL 400EX instrument. EDX spectra and electron diffraction patterns were obtained using a Philips CM20 microscope with a LINK-2000 attachment. The theoretical HREM images were simulated by means of the MacTempas software.

3. RESULTS

3.1. Synthesis and Sample Characterization

The results of the most representative syntheses are summarized in Table 1. X-ray diffraction pattern of sample 1 revealed the formation of a pure Ca_2MnGaO_5 compound with cell parameters clearly related to the cell parameters of perovskite: $a \approx c \approx a_{per}\sqrt{2}$, $b \approx 4a_{per}$. The reflections $0kl$, $k + l \neq 2n$, and $hk0$, $h \neq 2n$ were systematically absent, which allows us to propose the most symmetric space group *Pnma*. The cation composition of the Ca_2MnGaO_5 compound was verified by EDX analysis. The cation ratio Ca:Mn:Ga = 2.03(3):0.98(4):0.99(5) determined from seven crystallites is in good agreement with the Ca_2MnGaO_5 formula.

Ca_2MnGaO_5 can be prepared also by annealings in air or under N_2 flow. Increasing the partial oxygen pressure on going from the ampoule synthesis to annealing in air leads to higher temperature (1300°C instead of 1000°C) required for the successful formation of Ca_2MnGaO_5. The samples prepared by these techniques contain a small amount of an impurity phase ($\sim$2%) which also shows reflections related to the perovskite sublattice. Using X-ray diffraction we were unable to identify this impurity due to the small amount of admixture reflections and their low intensity; probably, it

TABLE 1
Cell Parameters, Mn Formal Valence, and Oxygen Content of $Ca_2MnGaO_{5+\delta}$ and $Ca_2MnGa_{1-x}Zn_xO_{5+\delta}$ for Different Preparation Conditions

No.	Initial compositions and treatment conditions	Cell parameters (Å)	V_{Mn}	δ
1	$Ca_2MnGaO_{5+\delta}$, synthesis in quartz ampoule (Technique 1)	$a = 5.2685(4)$ $b = 15.301(1)$ $c = 5.4686(5)$	+3.09	0.045
2	$Ca_2MnGaO_{5+\delta}$, synthesis in N_2 flow (Technique 2)	$a = 5.275(2)$ $b = 15.262(5)$ $c = 5.472(2)$	+3.18	0.09
3	$Ca_2MnGaO_{5+\delta}$, synthesis in air (Technique 3)	$a = 5.2712(7)$ $b = 15.267(1)$ $c = 5.4722(6)$	+3.18	0.09
4	$Ca_2MnGaO_{5+\delta}$ annealed under 80 atm O_2, 415°C, 15 h	$a = 5.302(1)$ $b = 14.940(4)$ $c = 5.428(2)$	+3.78	0.39
5	$Ca_2MnGa_{0.9}Zn_{0.1}O_{5+\delta}$, annealing in air at 1000°C for 48 h and 1200°C for 40 h	$a = 5.278(1)$ $b = 15.216(4)$ $c = 5.479(1)$	+3.25	0.075
6	$Ca_2MnGa_{0.8}Zn_{0.2}O_{5+\delta}$, annealing in air at 1000°C for 48 h and 1200°C for 40 h	$a = 5.278(1)$ $b = 15.163(5)$ $c = 5.486(1)$	+3.36	0.08

belongs to an anion-deficient perovskite with a disordered distribution of Ga and Mn cations.

It was found that the samples prepared in a silica tube (sample 1) and in N_2 flow or in air (samples 2 and 3) have significantly different cell parameters. We assume the variation of the cell dimensions to be related to the variable oxygen content in $Ca_2MnGaO_{5+\delta}$. The formal Mn valence determined by iodometric titration was found to be higher than +3, showing an excess of oxygen in $Ca_2MnGaO_{5+\delta}$ with $\delta = 0.045$ for sample 1 and $\delta = 0.09$ for samples 2 and 3. In order to investigate the range of oxygen nonstoichiometry in $Ca_2MnGaO_{5+\delta}$ additional annealings were performed under oxygen pressure varying from 1 atm (O_2 flow) to 80 atm at 415°C. Thermal treatment at $P(O_2) = 1$ atm does not lead to noticeable changes in cell parameters, whereas the oxidation at $P(O_2) = 80$ atm results in a decrease of the orthorhombic distortion and a contraction of the b parameter (sample 4). After this treatment a formal Mn oxidation state of $V_{Mn} = +3.78$ and $\delta = 0.39$ were achieved. Treatments at intermediate oxygen pressures 20 atm $< P(O_2) <$ 80 atm did not allow to prepare the compounds with intermediate oxygen content; instead the mixture of two brownmillerite-type compounds with $\delta \approx 0.4$ and $\delta \approx 0.1$, respectively, was formed at relatively short treatment duration (δ values were assigned from the determined cell parameters of the phases); prolonged oxidation yielded pure $\delta \sim 0.4$ compound. To prepare the brownmillerites with $+3.18 < V_{Mn} < +3.78$ heterovalent cation substitution was used with the replacement of Ga^{3+} cations by Zn^{2+}. $Ca_2MnGa_{1-x}Zn_xO_{5+\delta}$ solid solutions with $x = 0.1$ and $x = 0.2$ were prepared in air at 1200°C. The formal Mn valence increases with increasing Zn content ($V_{Mn} = +3.25$ ($x = 0.1$) and $V_{Mn} = +3.36$ ($x = 0.2$)), whereas the δ value remains approximately the same for both samples and is close to the δ obtained after annealing of $Ca_2MnGaO_{5+\delta}$ in air or in a N_2 flow.

3.2. *Crystal Structure*

The crystal structure of $Ca_2MnGaO_{5.045}$ was first refined from X-ray powder data. Starting atomic positions were taken from the $Ca_2Fe_2O_5$ structure (11). Attempts were made to localize extra oxygen atoms in the (GaO) layers, but difference Fourier syntheses did not reveal the presence of maxima which might correspond to oxygen atoms, probably due to the small amount of excess oxygen and its low scattering factor. The final refinement was performed with an isotropic approximation for the thermal parameters. The thermal parameter of the O3 oxygen atom in the (GaO) layer was found to be larger ($B_{iso}(O3) = 4.6$ Å^2) than B_{iso} for O1 and O2 atoms. The refinement of occupancy factor for the O3 atom yielded the value of 0.9(1). All oxygen atoms were finally treated with equal thermal parameters. Thermal parameters for cations were refined separately. After the final refinement good values for the reliability factors were obtained: $R_I = 0.025$, $R_P = 0.022$, $R_{wP} = 0.030$. Experimental,

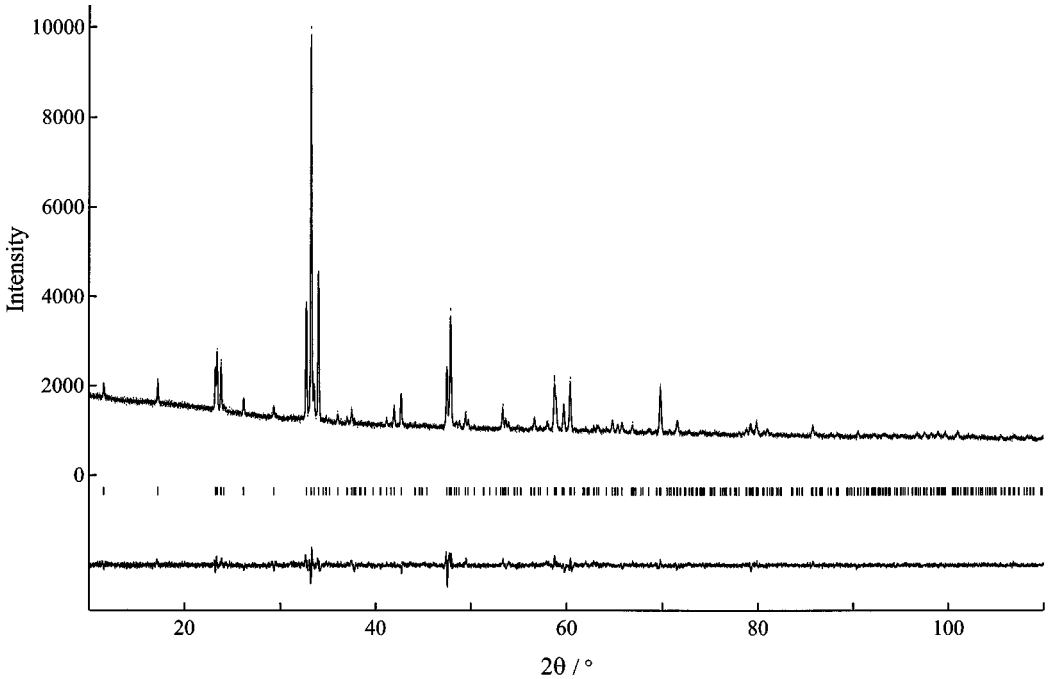

FIG. 1. Experimental and difference X-ray diffraction profiles for $Ca_2MnGaO_{5.045}$.

calculated, and difference X-ray powder patterns are shown in Fig. 1. The parameters of the refinement are given in Table 2. Atomic coordinates for $Ca_2MnGaO_{5.045}$ are listed in the first rows of the *Pnma* part of Table 3.

Anomalous behavior of B_{iso} for the O3 atom may indicate that the Rietveld refinement of the X-ray diffraction powder data only provides an approximate model of the crystal structure. Although the X-ray diffraction pattern for the $Ca_2MnGaO_{5.045}$ sample can be adequately fitted in a *Pnma* model, the description of the neutron diffraction data in this model is not perfect; reliability factors are $R_p = 6.24$, $R_{wp} = 8.19$, $\chi^2 = 10.1$. Most striking was the systematic underweight in the calculated intensity for the reflections with $h + k + l = 2n$ and the nonmonotonical behavior of the peak FWHM's with d spacings. We assume that this effect is caused by the presence of two different brownmillerite-based structures which, however, are very closely related and mainly differ by the symmetry relation between two adjacent ($GaO\square$) layers (Fig. 2). If the layers are connected by an inversion center, the structure adopts *Pnma* symmetry ($Ca_2Fe_2O_5$ (11)), as it was found for $Ca_2MnGaO_{5.045}$ by X-ray diffraction. In the case of a noncentrosymmetric space group *Ima*2 ($LaACuGaO_5$ (A = Ca, Sr) (8, 9), Ca_2FeAlO_5 (12)) the layers have the same orientation with respect to crystal axes but are shifted with respect to each other by additional translation due to the body-centered lattice. Using the notations described in details by Krekels *et al.* (13), the *Ima*2 phase can be represented as consisting of either R-type (right-hand chains) or L-type (left-hand chains) Ga–O chains only, whereas the *Pnma* phase is formed due to ordered –L–R–L–R– alternation along the *b* axis. The *Pnma*⇔*Ima*2 transformation does not essentially affect the coordination numbers, the interatomic distances, and the tilting pattern of the MnO_6 layers. Moreover, according to calculations performed (14,15), these two structures have nearly identical lattice energies and hence close probabilities of the formation may be assumed.

TABLE 2
Selected Parameters from Rietveld Refinement of X-Ray and Neutron Diffraction Powder Data for $Ca_2MnGaO_{5.045}$ Crystal Structure

	X-ray data	NPD data	
Space group	*Pnma*	*Pnma*	*Ima*2
a (Å)	5.26769(5)	5.2690(3)	15.231(2)
b (Å)	15.2928(2)	15.3003(9)	5.4783(9)
c (Å)	5.46785(6)	5.4671(3)	5.2722(8)
Z	4	4	4
Cell volume (Å^3)	440.478(8)	440.74(8)	439.9(2)
Calculated density (g/cm^3)	4.295	4.292	4.300
2θ Range, step, deg.	$10 \le 2\theta \le 110$,0.01	$6 \le 2\theta \le 125.7$,0.05	
No. of reflections	283	370	208
Refinable parameters	17	17	15
Mass fraction of the phases	—	0.82(2)	0.18(2)
R_I (χ^2), R_P, R_{wP}	2.53, 2.26, 3.04	6.75, 5.02, 6.63	

TABLE 3
Positional and Thermal Parameters of Atoms for $Ca_2MnGaO_{5.045}$ Determined from X-Ray Powder Refinement (*Pnma* (First Rows)) and Neutron Powder Refinement (*Pnma* (Second Rows) and *Ima*2)

Atom	Position	Occupancy	*x*/*a*	*y*/*b*	*z*/*c*	B_{iso} (Å^2)
			Pnma			
Ca	8*d*	1	0.4903(9)	0.1095(1)	0.0236(5)	0.88(7)
		1	0.4875(8)	0.1107(3)	0.0225(8)	0.47(5)
Mn	4*a*	1	0	0	0	0.30(8)
		1	0	0	0	1.2(1)
Ga1	4*c*	1	0.4724(8)	$\frac{1}{4}$	0.5652(4)	1.41(9)
		0.89(2)	0.4543(9)	$\frac{1}{4}$	0.5667(8)	0.96(6)
Ga2	4*c*	—	—	—	—	—
		1-g(Ga1)	1-*x*(Ga1)	$\frac{1}{4}$	*z*(Ga1)	B(Ga1)
O1	8*d*	1	0.248(7)	0.9886(4)	0.238(2)	1.6(1)
		1	0.2588(8)	0.9879(2)	0.2394(6)	0.70(2)
O2	8*d*	1	0.017(2)	0.1470(4)	0.067(1)	B(O1)
		1	0.0251(7)	0.1441(2)	0.0668(7)	B(O1)
O3	4*c*	1	0.602(2)	$\frac{1}{4}$	0.877(2)	B(O1)
		g(Ga1)	0.5897(8)	$\frac{1}{4}$	0.8825(8)	B(O1)
O4	4*c*	—	—	—	—	—
		1-g(Ga1)	1-*x*(O3)	$\frac{1}{4}$	*z*(O3)	B(O1)
			*Ima*2			
Ca	8*c*	1	0.112(1)	0.018(4)	0.515(3)	0.5
Mn	4*a*	1	0	0	0.062(7)	B(Ca)
Ga1	4*b*	1	$\frac{1}{4}$	0.928(4)	0.047(5)	B(Ca)
O1	8*c*	1	0.989(1)	0.258(3)	0.249(4)	0.70(2)
O2	8*c*	1	0.141(1)	0.066(3)	0.968(5)	B(O1)
O3	4b	1	$\frac{1}{4}$	0.641(3)	0.161(5)	B(O1)

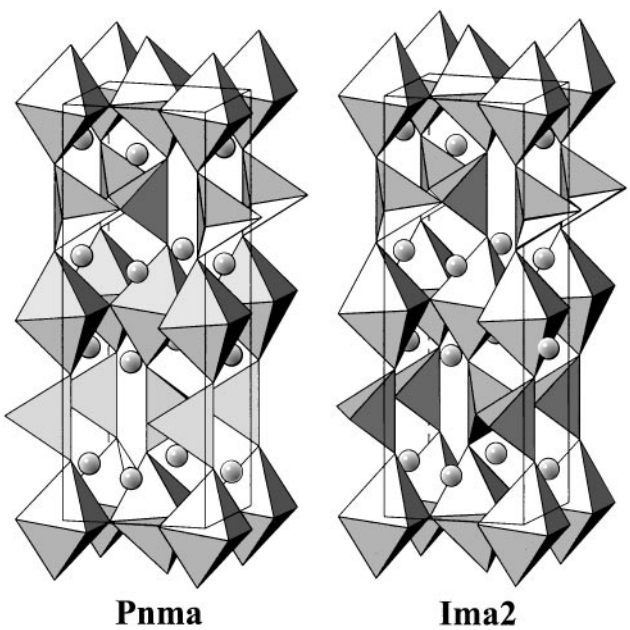

FIG. 2. Comparison of two brownmillerite-type structures with *Pnma* and *Ima*2 space symmetry. Mn atoms are located within the octahedra, tetrahedra are occupied by Ga cations. Ca atoms are imaged as spheres.

Therefore, a second phase with *Ima*2 symmetry was introduced into the refinement. This yielded a much better description of diffraction profile, although the reliability factors values are still quite high ($R_p = 5.14$, $R_{wp} = 6.76$, $\chi^2 = 6.91$). A fit of the most representative part of the spectrum in *Pnma* and in a two-phase model is presented in Fig. 3. The refined fraction of *Ima*2 phase is 18(2)%. Some other *I*-centered space groups (*Imcm* and *I*2*cm*) were checked; however, they all provide the description of the spectrum worse than the *Pnma* + *Ima*2 model.

Difference Fourier syntheses were performed based on the structure factors obtained from the profile matching of the NPD data with the use of the SHELX-97 software. The presence of the *Ima*2 phase was ignored and the profile approximation was performed under the assumption that the diffraction intensities are produced by *Pnma* phase only. The strongest maximum has coordinates (0.585, 1/4, 0.875). The Fourier map calculated from data with the O3 atom removed yielded two maxima with intensity ratio 1.22:1. The former maximum position is coincident with the actual O3 position of the standard *Pnma* model, while the latter position is the same as that from the primary synthesis. These positions suggest the model in which two orientations of Ga–O chains are intermixed within the *Pnma* phase (Fig. 4). The position of Fourier maximum O4 is exactly

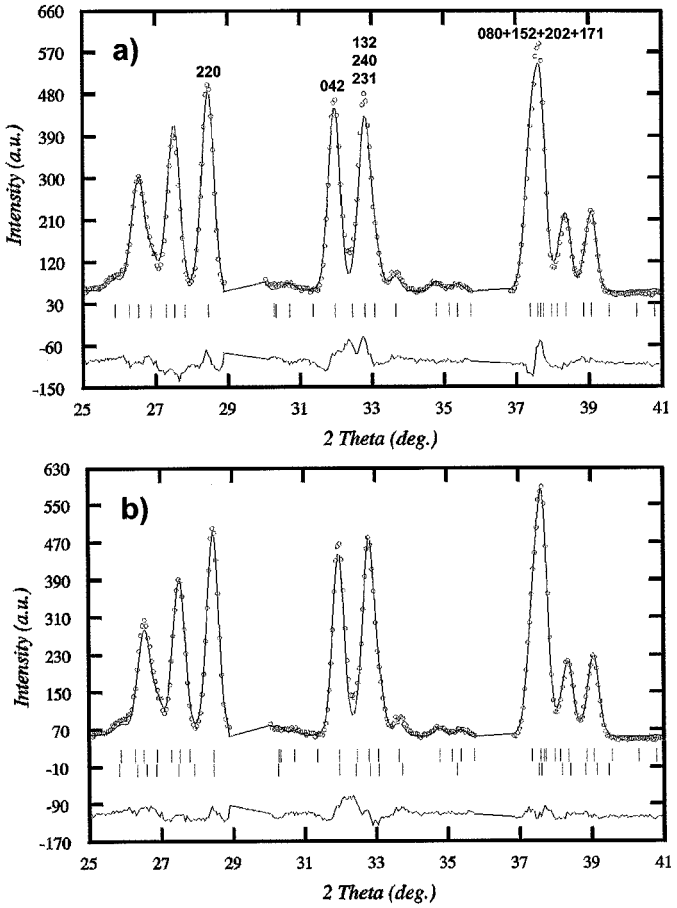

FIG. 3. Fitting of the neutron diffraction profile using the single-phase *Pnma* model (a) and the two-phase (*Pnma* and *Ima*2) model (b). Note the systematic underweight of the intensities of the $h + k + l = 2n$ reflections (a).

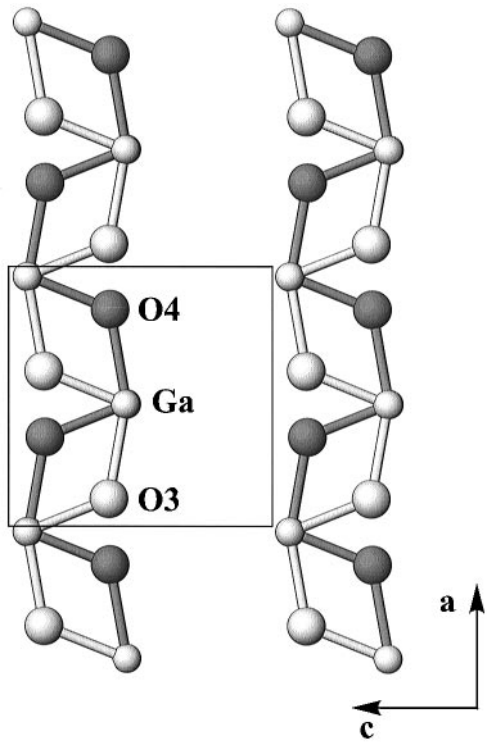

FIG. 4. Scheme illustrating the splitting of the O3 and O4 atoms due to a different orientation of the Ga–O chains. Two possible configurations are distinguished by a different shading intensity. For clarity, the splitting of the Ga atoms is not shown.

what was expected to originate from the *Ima*2 impurity. The combination of the above NPD data with HREM observations described below shows that the actual structure of the material can be represented as follows: *Ima*2 fragments occur on two length scales: on the one hand, they form separate crystallites and, on the other hand, microdomains of *Ima*2 symmetry occur within *Pnma* matrix, visualized as different Ga–O chain orientations in *Pnma* blocks.

To maintain reasonable interatomic distances between Ga and splitted O3 and O4 atoms splitting of the Ga-position was also introduced. The fractions of split O and Ga positions were fixed to each other and their refined values are $g_1 = 0.89$, $g_2 = 0.11$. Final reliability factors are $R_p = 5.02$, $R_{wp} = 6.63$, $\chi^2 = 6.75$. Refined parameters for the model described above are listed in Tables 2 and 3. The main interatomic distances are presented in Table 4. The introduction of a common occupation of the *B* sites by Mn and Ga atoms does not lead to a better fit of the diffraction profile, and the refined value of $Ga_{Mn} = Mn_{Ga} \sim 1\%$, which is within the error limit, so the effect is negligible, if present at all. These data are of high reliability because of large difference in atomic scattering factors for Ga (0.729) and Mn (-0.373).

Relatively high *R* factor values and slightly asymmetric description of some group of reflections (e.g., the fit of (240) (in *Pnma* setting) reflection is nearly perfect, while the (042) one has still discrepancy between experimental and calculated intensities) indicate that there can exist some other factors not introduced in the model accepted. Although

TABLE 4
Selected Interatomic Distances in the *Pnma* Structure of $Ca_2MnGaO_{5.045}$ (Å) Calculated from the NPD Data

Ca–O1	2.472(6) × 1	Mn–O1	1.899(4) × 2
Ca–O1	2.521(6) × 1	Mn–O1	1.918(4) × 2
Ca–O1	2.528(6) × 1	Mn–O2	2.239(3) × 2
Ca–O1	2.696(6) × 1	Ga1–O2	1.816(4) × 2
Ca–O2	2.311(6) × 1	Ga1–O3	1.868(6) × 1
Ca–O2	2.501(6) × 1	Ga1–O3	1.941(6) × 1
Ca–O2	2.889(6) × 1	Ga2–O2	1.780(4) × 2
Ca–O3[a]	2.328(5) × 1	Ga2–O4	1.868(6) × 1
Ca–O4[a]	2.301(5) × 1	Ga2–O4	1.941(6) × 1

[a] Either Ca–O3 or Ca–O4, only one can be present.

further refinements are obviously possible we suppose they would be of low reliability. The possible improvements may include the effect of stacking faults arising from random intermixing of *Pnma*/*Ima*2 domains. Also the off-stoichiometric (corresponding to $\delta = 0.045$) oxygen atom position has not been determined since no extra maxima were observed on difference Fourier patterns.

$Ca_2MnGaO_{5.045}$ has a typical brownmillerite structure consisting of alternating (MnO_2), (CaO), and ($GaO\square$) layers. The Jahn–Teller effect, which is inherent for Mn^{3+} cations, leads to significant deformations of the coordination polyhedra in the $Ca_2MnGaO_{5.045}$ crystal structure. The MnO_6 octahedron is characterized by four short equatorial Mn–O distances (1.899 and 1.918 Å) and two long apical ones (2.239 Å), oriented along the *b* axis in the *Pnma* space group. Oxygen tetrahedra around the Ga atoms are slightly compressed along the *b* axis. The Ca cations are located in the 10-fold coordination polyhedra, but two Ca–O bonds of 3.268–3.796 Å are noticeably longer compared to the eight bonds ranging between 2.311 and 2.889 Å.

The crystal structures of the $Ca_2MnGaO_{5.39}$ and $Ca_2MnGa_{0.8}Zn_{0.2}O_{5.08}$ were refined from X-ray powder data using the *Pnma* structure model. The refinements gave good correspondence between experimental and calculated X-ray profiles ($R_I = 0.027$ (0.029), $R_P = 0.014$ (0.022), $R_{wP} = 0.019$ (0.029) for the $Ca_2MnGaO_{5.39}$ ($Ca_2MnGa_{0.8}Zn_{0.2}O_{5.08}$) structures). However, the atomic positions and interatomic distances obtained during the refinements probably reflect only an approximate model whereas the real structure could be more complicated as it was found by neutron diffraction for $Ca_2MnGaO_{5.045}$. Nevertheless, these data were used to reveal the structure changes in the investigated compounds upon the variation of formal Mn valence. The vanishing of the average Jahn–Teller deformation in the MnO_6 octahedra follows the increase of the formal Mn valence. In the $Ca_2MnGa_{0.8}Zn_{0.2}O_{5.08}$ structure ($V_{Mn} = +3.36$) Mn cations have an almost square equatorial environment (d(Mn–O1) = 1.91(1) and 1.93(1) Å). The apical Mn–O(2) separation is contracted from 2.239 Å in $Ca_2MnGaO_{5.045}$ to 2.221(9) Å in $Ca_2MnGa_{0.8}Zn_{0.2}O_{5.08}$ and 1.873(9) Å in $Ca_2MnGaO_{5.39}$. In the latter case the MnO_6 octahedron is "apically compressed" with the apical Mn–O distance being equal or shorter than the equatorial ones. The equatorial Mn–O1 bonds in $Ca_2MnGaO_{5.39}$ remain non-equivalent (d(Mn–O1) = 1.87(2) and 1.94(3) Å). The increase of the amount of Mn^{4+} cations is accompanied by a decrease of the average $\langle$Mn–O$\rangle$ distance from 2.02 Å in $Ca_2MnGaO_{5.045}$ to 1.89 Å in $Ca_2MnGaO_{5.39}$, in agreement with the ionic radii of Mn^{3+} ($r = 0.65$ Å) and Mn^{4+} ($r = 0.54$ Å) in an octahedral environment.

Using X-ray powder diffraction we were unable to determine the position of the extra oxygen atoms even in case of $Ca_2MnGaO_{5.39}$ compound, which contains a relatively large amount of excess oxygen atoms. Moreover, the thermal parameters for the Ga and O3 atoms were found to be abnormally high. It is reasonable to suppose that extra oxygen atoms occupy vacant anion positions in ($GaO\square$) layers, which results in an increase of the coordination number of Ga with large displacements of all atoms in ($GaO_{1+x}\square_{1-x}$) layers. To reveal the structural changes

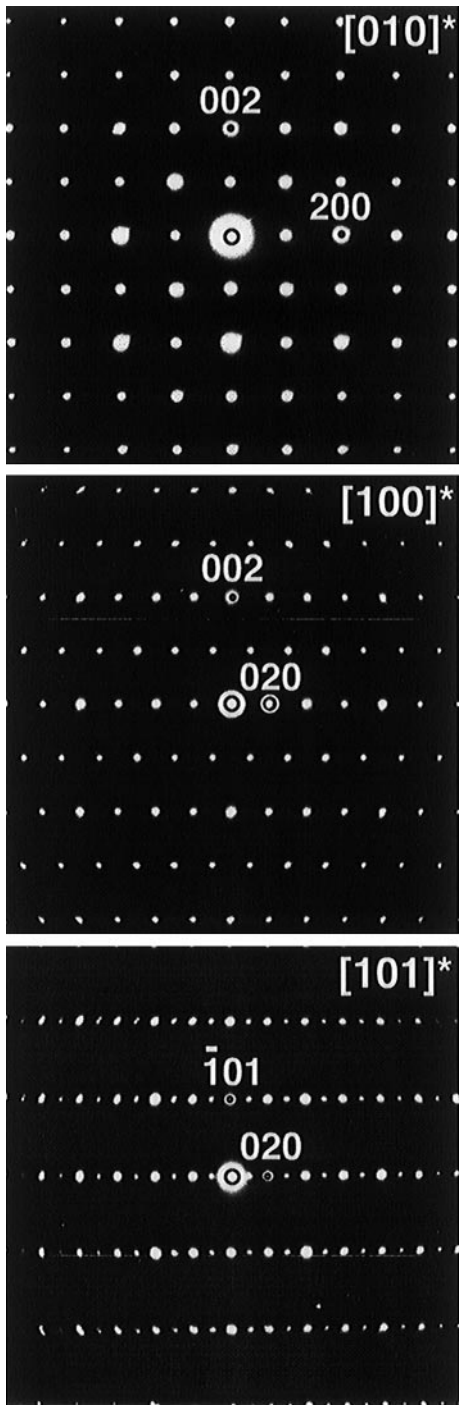

FIG. 5. [010]*, [100]*, and [101]* electron diffraction patterns of $Ca_2MnGaO_{5.045}$.

under oxidation we performed electron microscopy of $Ca_2MnGaO_{5.045}$ and $Ca_2MnGaO_{5.39}$ compounds.

3.3. Electron Microscopy Investigation

3.3.1. $Ca_2MnGaO_{5.045}$. Some low-order zone electron diffraction (ED) patterns of the $Ca_2MnGaO_{5.045}$ compound are shown in Fig. 5. ED patterns of the [010]* and [101]* zones exhibit $h00$, $h \neq 2n$, $00l$, $l \neq 2n$ and $0k0$, $k \neq 2n$ reflections forbidden by the *Pnma* symmetry. The intensity of forbidden reflections decreases drastically with crystal tilt, which allows us to attribute them to double diffraction. Indeed, the $0kl$, $k + l \neq 2n$ reflections are absent in the [100]* pattern. ED patterns therefore confirm the *Pnma* symmetry.

High-resolution (HREM) images along [100] or [101] (Fig. 6) show the layered brownmillerite structure. The perovskite sublattice can be recognized as the square dot pattern along the [101] zone, which corresponds to [100] projection of the perovskite subcell. ($GaO\square$) layers appear as rows of less bright dots repeated each fourth layer and exhibiting a periodicity of 15.3 Å. This periodicity is more strongly pronounced in thicker areas (right part of Fig. 6). Calculated images of [100] and [101] zones for different defocus values and thicknesses are in good agreement with the experimental HREM images; they are shown in Fig. 7.

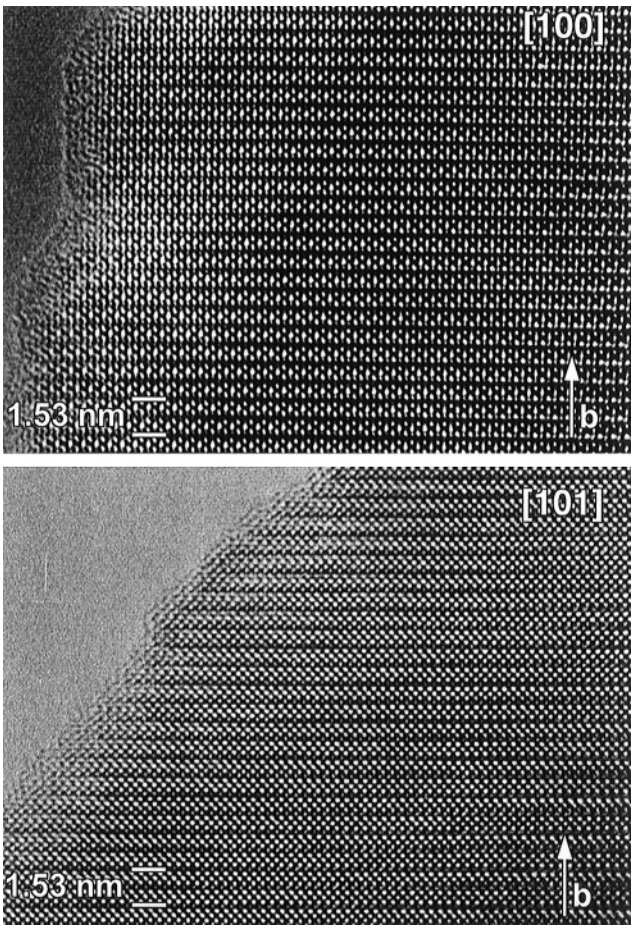

FIG. 6. [100] and [101] HREM images of $Ca_2MnGaO_{5.045}$ showing the perfect brownmillerite structure.

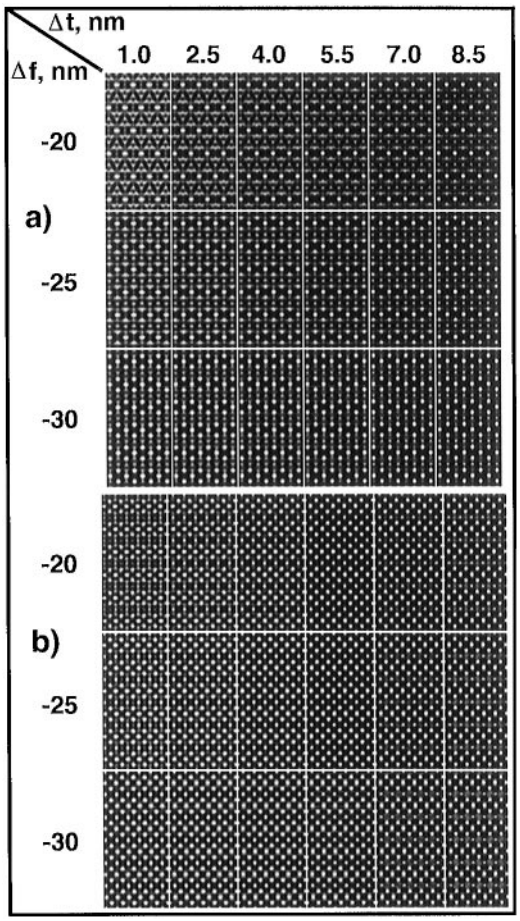

FIG. 7. Matrix of calculated [100] (a) and [101] (b) HREM images using structure data from the X-ray Rietveld refinement of $Ca_2MnGaO_{5.045}$. The images are to be compared with the experimental ones from Fig. 6.

The [101]* ED patterns often exhibit an intensity variation of the hkl, $k \neq 2n$ reflections between different crystallites, even between different areas of the same crystallite. According to the results of the NPD refinement, this can be related to the presence of both the *Pnma* and the *Ima*2 phases. HREM observations indeed confirm the presence of *Pnma* and *Ima*2 domains in $Ca_2MnGaO_{5.045}$. Figure 8 shows [101] HREM images and corresponding computer simulated Fourier transforms of the crystallites exhibiting the *Pnma* (a, b) and the *Ima*2 (c, d) structures, respectively. The Fourier transform corresponding to *Pnma* symmetry (Fig. 8a) clearly demonstrates hkl, $k \neq 2n$ spots, which are forbidden by *Ima*2 symmetry and which are absent on the corresponding Fourier transform pattern (Fig. 8c). The

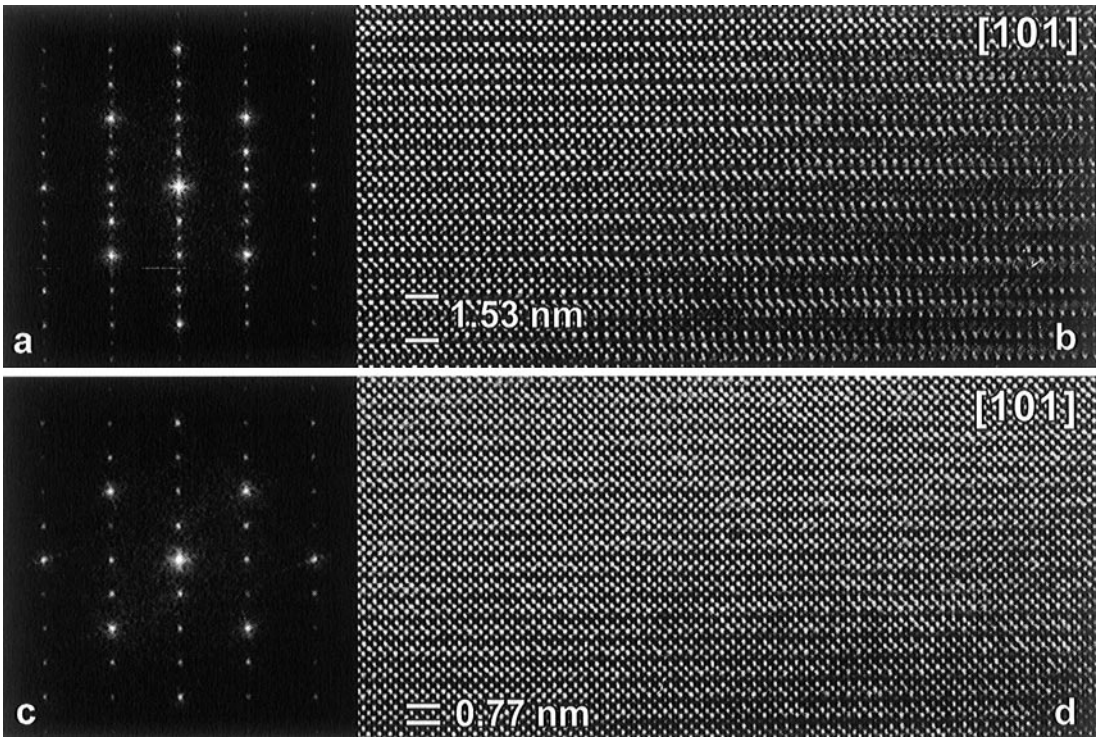

FIG. 8. [101] HREM images and corresponding Fourier transform patterns of domains of well-ordered *Pnma* (a, b) and *Ima*2 (c, d) phases in $Ca_2MnGaO_{5.045}$. The visible repeat period for the *Pnma* phase is twice that for the *Ima*2 phase.

Pnma structure can also be distinguished in the HREM image by the periodicity of 15.3 Å along the *b* axis (Fig. 8b), whereas the visible repeat period of the *Ima*2 phase is two times shorter (Fig. 8d). Apart from crystallites exhibiting either the pure *Pnma* or the pure *Ima*2 structure, areas were also found where both phases are closely intermixed and form domains with variable thicknesses alternating along the *b* axis (Fig. 9). This observation favors the assumption that the splitting of the Ga and O3 positions observed by neutron diffraction results from a violation of the perfect stacking sequence of ($GaO\square$) layers. It also causes a streaking of the *hkl*, $k \neq 2n$ reflections and the appearance of satellite reflections when *Pnma* and *Ima*2 blocks form a quasiperiodic arrangement. Occasionally, [101]* ED patterns were found that demonstrate satellites with $q^* = 1/9b^*$, which probably corresponds to an ordered alternation of *Pnma* and *Ima*2 blocks with the width of 4 and 5 unit cells.

It is a typical feature of complex oxides (and especially for CMR manganites) that crystal structure refinement by means of X-ray powder data yields only an average representation of the actual structure. In the present case X-ray diffraction patterns can be adequately fitted assuming a simple *Pnma* model and further details are unveiled by electron and neutron diffraction combined with high-resolution electron microscopy, the reason being that the corresponding structural features involve almost exclusively oxygen atom positions. Both features discovered (the presence of the *Ima*2 phase and the splitting of the oxygen position within *Pnma*) represent different possibilities of the Ga–O chain orientation, which are energetically very close. The actual crystal structure consists of a complicated intermixture of blocks with different structures.

3.3.2. $Ca_2MnGaO_{5.39}$. The [010]* ED pattern of $Ca_2MnGaO_{5.39}$ exhibits a noticeable difference in comparison with the same diffraction pattern for the reduced material (Fig. 10). The intensity of the $h0l$, $h + l \neq 2n$ reflections is drastically decreased for the oxygenated material. This indicates the suppression of the $a \approx c \approx a_{per}\sqrt{2}$ superstructure by the insertion of extra oxygen atoms at the vacant positions in the ($GaO\square$) layers. This eliminates the structure deformations characteristic for the $Ca_2MnGaO_{5.045}$ material due to ordering of the oxygen atoms and anion vacancies in the ($GaO\square$) layers and the cooperative tilt of the MnO_6 octahedra. A similar transformation was observed before in fluorinated brownmillerite $LaSrCuGaO_5$ (16), where the insertion of additional anions into the ($GaO\square$) layers causes a transition from an orthorhombic structure with $a \approx c \approx a_{per}\sqrt{2}$ supercell to a tetragonal one with $a \approx a_{per}$. The decrease of the orthorhombic distortion after oxidation can be noticed on the [010]* ED pattern. The c/a ratio measured from the ED pattern is equal to 0.976 in accordance with the value found by X-ray diffraction for oxygenated material ($c/a = 0.977$).

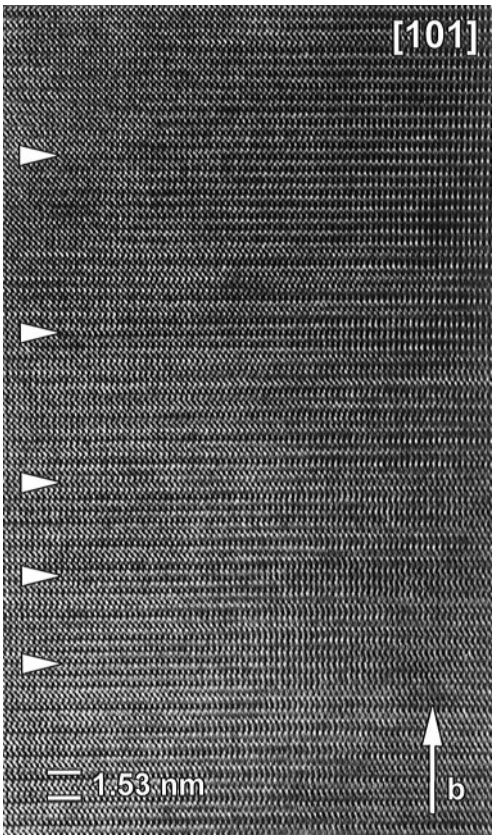

FIG. 9. [101] HREM image of an area with a disordered alternation of *Pnma* and *Ima*2 domains with different width. The *Ima*2 domains are marked by arrowheads.

The elongation of the spots along the b^* was observed on [001]* and [101]* ED patterns of the oxygenated material (Fig. 10). In fact, this elongation arises from the presence of satellite spots positioned very close to the basic reflections; it could be observed from the [101]* ED pattern at greater magnification. However, the origin of these satellite reflections in $Ca_2MnGaO_{5.39}$ is essentially different from that in the $Ca_2MnGaO_{5.045}$ compound. The [101] HREM image shows that insertion of oxygen affects significantly the ($GaO\square$) layers (Fig. 11). Each second Ga-containing layer exhibits a contrast, which is nearly identical to the contrast produced by the two neighboring MnO_2 layers. It is reasonable to assume that only half of the ($GaO\square$) layers adopt extra oxygen atoms, transforming into a (GaO_2) layers, whereas the other ($GaO\square$) layers remain unaffected. The ($GaO\square$) and (GaO_2) layers alternate in an ordered manner but the perfect stacking is occasionally violated by slabs with an *Ima*2 structure (marked by a bracket in Fig. 11). The longest parameter for the *Ima*2 slabs has a value of 15.3 Å, which is larger than the corresponding cell dimension in areas of alternating ($GaO\square$) and (GaO_2) layers (14.9 Å) and probably reflects lower oxygen content within these slabs.

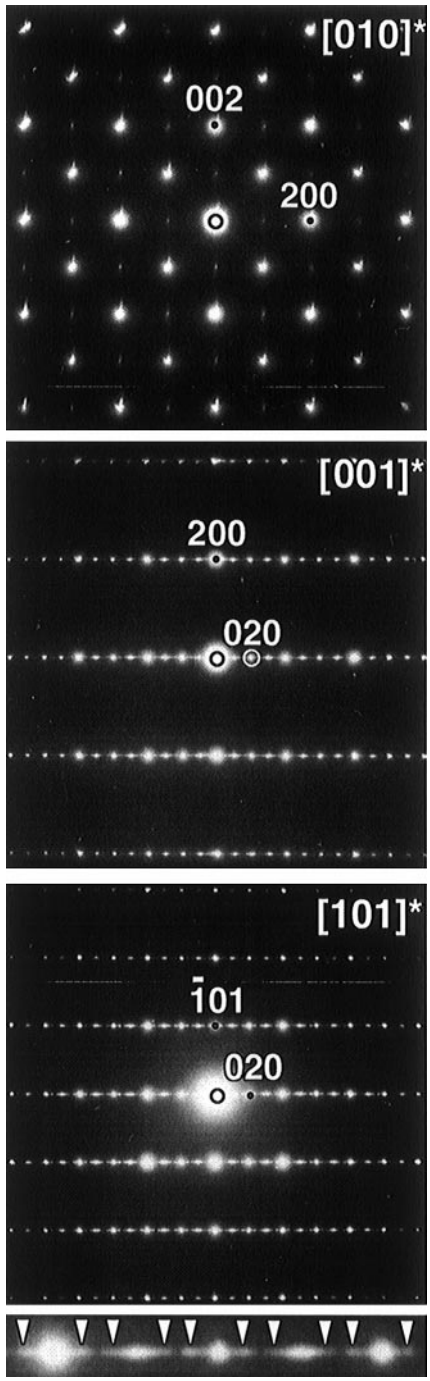

FIG. 10. [010]*, [001]*, and [101]* electron diffraction patterns for $Ca_2MnGaO_{5.39}$. The weakness of the $h0l$, $h + l \neq 2n$ spots on the [010]* pattern can be noticed by comparing with the [010]* pattern of Fig. 5. Note also the elongation of spots along the b^* on [001]* and [101]* patterns. The enlargement shows that this elongation is caused by the presence of extra reflections.

The *Ima*2 slabs and the slabs of oxygenated material may periodically alternate along the long axis, causing the appearance of satellites on ED patterns. Upon intense

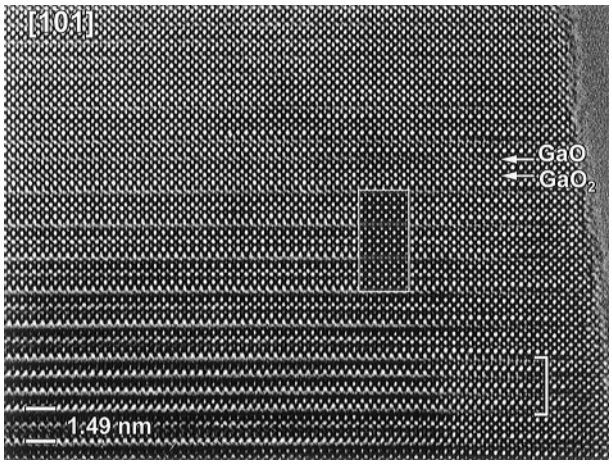

FIG. 11. [101] HREM image of $Ca_2MnGaO_{5.39}$ material. The ($GaO\square$) and (GaO_2) layers are marked. The *Ima*2 slab is marked by bracket. The image, calculated using $Ca_2MnGaO_{5.5}$ model ($\Delta f = -600$ Å, $t = 30$Å), is shown in the inset.

electron irradiation, the specific microstructure of the $Ca_2MnGaO_{5.39}$ transforms into an *Ima*2 structure. The transformation is accompanied by an expansion of the unit cell along the *b* axis and a decrease of the intensity of *hkl*, $k \neq 2n$ spots. This can be attributed to a loss of oxygen under beam irradiation and a local heating of the sample in the vacuum of the microscope column.

The idealized structure of the oxygenated material can be represented by the stacking sequence $-GaO_2-CaO-MnO_2-CaO-GaO\square-CaO-MnO_2-CaO-GaO_2-$ as shown in Fig. 12. The two neighboring Ga–O layers are no longer symmetrically connected in this structure. It can be described within the $a \approx 4a_{per}$, $b \approx c \approx a_{per}\sqrt{2}$ unit cell with $Pmc2_1$ space group which is a noncentrosymmetric subgroup of *Pnma*. Ga atoms in the (GaO_2) layers are octahedrally coordinated by six oxygen atoms. This idealized oxygenated phase has the $Ca_2MnGaO_{5.5}$ composition, which agrees with the oxygen nonstoichiometry $\delta = 0.39$ if the presence of some reduced *Ima*2 blocks is taken into account. The HREM simulated image shown as an inset in Fig. 11 and calculated using this model ($\Delta f = -600$ Å, $t = 30$ Å) shows remarkable agreement with the experimental image.

4. DISCUSSION

The present study allows us to assume that the synthesis conditions stabilizing Mn with formal valence close to +3 (low partial oxygen pressure and high annealing temperature) are favorable for formation of a layered brownmillerite structure with an ordered distribution of Ga and Mn cations among the *B* positions. The ordering of *B* cations clearly requires distinct crystallographic properties as it occurs for Mn^{3+} and Ga^{3+} cations. The former has a Jahn–Teller deformed octahedral environment whereas the latter is usually surrounded by a tetrahedron of four oxygen atoms. The apical elongation of the MnO_6 octahedra is an essential prerequisite for the formation of a layered structure. Insertion of oxygen atoms results in an increase of the coordination number for Ga and an increase

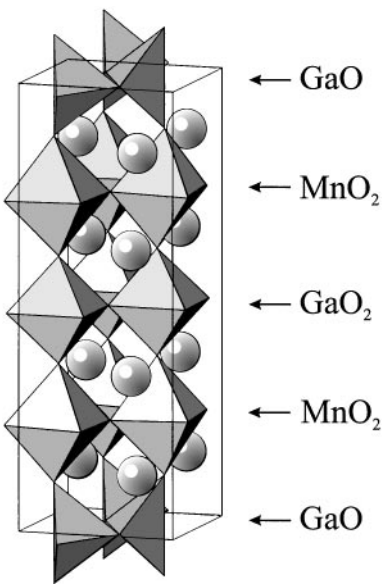

FIG. 12. Structure model of the fully oxidized $Ca_2MnGaO_{5.5}$ phase.

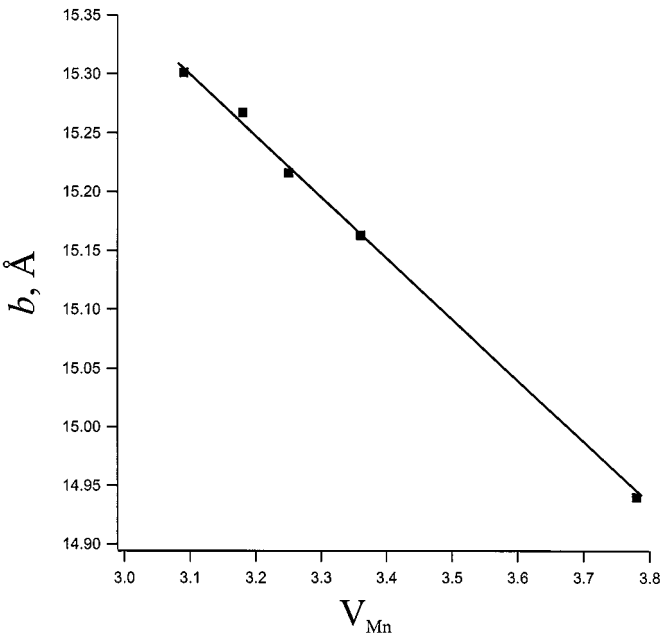

FIG. 13. Dependence of the *b* parameter vs the formal Mn oxidation state V_{Mn} for the $Ca_2MnGaO_{5+\delta}$ and $Ca_2MnGa_{1-x}Zn_xO_{5+\delta}$ compounds.

of the Mn formal valence, suppressing the Jahn–Teller distortion. This creates the possibility for a statistical distribution of Ga and Mn over the *B*-positions and the formation of disordered 3D perovskites. The Mn formal valence value probably restricts also the homogeneity range of the $Ca_2MnGa_{1-x}Zn_xO_{5+\delta}$ solid solution to $x = 0.2$. At the same time, the low value of δ makes it possible to preserve the tetrahedral coordination for the Ga atoms. All as-prepared materials including the Zn-substituted phases have only a small excess of oxygen ($0.045 \leq \delta \leq 0.09$).

The oxidation of as-prepared material drastically influences the crystal structure. The samples oxidized by oxygen insertion and heterovalent cation replacement show a *b*-parameter value linearly depending on the Mn formal oxidation state (Fig. 13). The contraction of the unit cell along the *b*-axis occurs due to the apical compression of the MnO_6 octahedra because of the suppression of the Jahn–Teller deformation on going from a high-spin d^4 to a d^3 electron configuration when V_{Mn} increases.

The intercalation of oxygen leads to a decrease of the orthorhombic distortion when comparing the *a* and the *c* cell parameters for $Ca_2MnGaO_{5.045}$ and $Ca_2MnGaO_{5.39}$. The reason for this behavior was recently described for fluorinated copper-based brownmillerite $LaACuGaO_5$ (A = Ca, Sr) (16). However, the fluorination of LaA-$CuGaO_5$ results in fluorine incorporation into all ($GaO\square$) layers, whereas in the $Ca_2MnGaO_{5.39}$ structure the (GaO_2) layers with fully occupied anion positions and anion-deficient ($GaO\square$) layers are present. The structure of the oxygenated $Ca_2MnGaO_{5.5} = Ca_4(Mn_2Ga)GaO_{11}$ compound may be considered as the third member of the brownmillerite $A_nB_{n-1}B'O_{3n-1}$ ($n = 4$) homologous series, in which three layers of BO_6 ($B_3 = Mn_2Ga$) octahedra form blocks separated by single layers of $B'O_4$ (B = Ga) tetrahedra. The oxidation state of Mn is equal to $+4$ in $Ca_2MnGaO_{5.5}$, but in the sample areas are present where δ is close to the value in the initial nonoxidized material and $V_{Mn} \approx +3$. This agrees well with the fact that the variation of $P(O_2)$ does not make it possible obtain a brownmillerite compound with an intermediate Mn oxidation state, but results in either a full oxidation or a mixture of reduced and oxidized phases.

The preliminary investigation of the reduced $Ca_2MnGaO_{5.045}$ compound revealed that it undergoes antiferromagnetic transition with $T_N = 165$ K. The detailed magnetic structure of the $Ca_2MnGaO_{5.045}$ compound as well as the magnetic properties of the oxidized $Ca_2MnGaO_{5.39}$ phase and $Ca_2MnGa_{1-x}Zn_xO_{5+\delta}$ solid solutions are under investigation and will be published elsewhere.

ACKNOWLEDGMENTS

This work was done with the help of the RFBR Program (Project 00-02-16736), SNSF Foundation (Grant 7SUPJ062190.00), CRDF Project 6559, and Program IUAP 4/10 of the Belgium government. M.V.L. is also grateful to the ICDD (2000 Crystallography Scholarship Award). The authors are grateful to V. Yu Pomyakushin and A. V. Olenev for helpful discussions.

REFERENCES

1. A. P. Ramirez, *J. Phys. Condensed Matter* **9,** 8171 (1997).
2. R. Mahesh, R. Mahendiran, A. K. Raychaudhury, and C. N. R. Rao, *J. Solid State Chem.* **122,** 448 (1996).
3. A. Maignan, C. Martin, G. Van Tendeloo, M. Herview, and B. Raveau, *J. Mater. Chem.* **8,** 2411 (1998).
4. J. M. Tarascon, Y. LePage, W. R. McKinnon, E. Tselepis, P. Barboux, B. G. Bagley, and R. Ramesh, *Mater. Res. Soc. Symp. Proc.* **156,** 317 (1989).
5. J. M. Tarascon, Y. LePage, W. R. McKinnon, R. Ramesh, M. Eibschutz, E. Tselepis, E. Wang, and G. W. Hull, *Physica C* **167,** 20 (1990).
6. M. Herview, C. Michel, D. Pelloquin, A. Maignan, and B. Raveau, *J. Solid State Chem.* **132,** 420 (1997).
7. T. P. Beales, M. Mölgg, J. R. Gorton, and D. C. Sinclair, *Mater. Res. Bull.* **31,** 1543 (1996)
8. A. L. Kharlanov, E. V. Antipov, I. Bryntse, A. V. Luzikova, and L. M. Kovba, *Eur. J. Solid State Inorg. Chem.* **29,** 1041 (1992).
9. A. V. Luzikova, A. L. Kharlanov, E. V. Antipov, and Hk. Muller-Bushbaum, *Z. Anorg. Allg. Chem.* **620,** 326 (1994).
10. F. Izumi, *in* "The Rietveld Method" (R. A. Young, Ed.), Chap. 13. Oxford Univ. Press, Oxford, 1993.
11. A. A. Collville, *Acta Crystallogr. B* **26,** 1469 (1970).
12. A. A. Collville and S. Geller, *Acta Crystallogr. B* **27,** 2311 (1971).
13. T. Krekels, O. Milat, G. Van Tendeloo, S. Amelinckx, T. G. N. Babu, A. J. Wright, and C. Greaves, *J. Solid State Chem.* **105,** 313 (1993).
14. R. Hoppe, *Angew. Chem.* **78,** 52 (1966).
15. R. Hoppe, *Adv. Fluorine Chem.* **6,** 387 (1972).
16. J. Hadermann, G. Van Tendeloo, A. M. Abakumov, B.Ph. Pavlyuk, M. Rozova, and E. V. Antipov, *Int. J. Inorg. Mater.* **2,** 493 (2001).